

# Improved Cation Binding to Lipid Bilayer with Negatively Charged POPS by Effective Inclusion of Electronic Polarization

Josef Melcr,<sup>\*,†,‡</sup> Tiago M. Ferreira,<sup>¶</sup> Pavel Jungwirth,<sup>§</sup> and O. H. Samuli Ollila<sup>\*,§,||</sup>

<sup>†</sup>*Institute of Organic Chemistry and Biochemistry of the Czech Academy of Sciences,  
Flemingovo nám. 542/2, CZ-16610 Prague 6, Czech Republic*

<sup>‡</sup>*Groningen Biomolecular Sciences and Biotechnology Institute and The Zernike Institute  
for Advanced Materials, University of Groningen, 9747 AG Groningen, The Netherlands*

<sup>¶</sup>*NMR group - Institut for Physics, Martin-Luther University Halle-Wittenberg*

<sup>§</sup>*Institute of Organic Chemistry and Biochemistry, Czech Academy of Sciences, Prague 6,  
Czech Republic*

<sup>||</sup>*Institute of Biotechnology, University of Helsinki*

E-mail: melcr@marge.uochb.cas.cz; samuli.ollila@helsinki.fi

## Abstract

Phosphatidylserine (PS) lipids are important signaling molecules and the most common negatively charged lipids in eukaryotic membranes. The signaling can be often regulated by calcium, but its interactions with PS headgroups are not fully understood. Classical molecular dynamics (MD) simulations can potentially give detailed description of lipid-ion interactions, but the results strongly depend on the used force field. Here, we apply the electronic continuum correction (ECC) to the Amber Lipid17 parameters of 1-palmitoyl-2-oleoyl-*sn*-glycero-3-phospho-L-serine (POPS) lipid to improve its interactions with K<sup>+</sup>, Na<sup>+</sup> and Ca<sup>2+</sup> ions. The partial charges of headgroup,

glycerol backbone and carbonyls of POPS, bearing a unit negative charge, were scaled with a factor of 0.75, derived for monovalent ions and the Lennard-Jones  $\sigma$  parameters of the same segments were scaled with a factor of 0.89. The resulting ECC-POPS model gives more realistic interactions with  $\text{Na}^+$  and  $\text{Ca}^{2+}$  cations than the original Amber Lipid17 parameters, when validated using headgroup order parameters and the "electrometer concept". In ECC-lipids simulations, populations of complexes of  $\text{Ca}^{2+}$  cations with more than two PS lipids are negligible, and interactions of  $\text{Ca}^{2+}$  cations with only carboxylate groups is twice more likely than with only phosphate groups, while interactions with carbonyls almost entirely involve also other groups. Our results pave the way for more realistic MD simulations of biomolecular systems with anionic membranes allowing to elucidate signaling processes involving PS and  $\text{Ca}^{2+}$ .

## 1 Introduction

Phosphatidylserine (PS) lipids are the most common negatively charged lipids in eukaryotic membranes and important signaling molecules<sup>1–3</sup>. They interact with signaling proteins<sup>2</sup>, regulate surface charge and protein localization<sup>4</sup>, induce protein aggregation<sup>5,6</sup> and membrane fusion<sup>7–9</sup>. As such lipid-related functions are also often regulated by ions<sup>2</sup>, a detailed understanding of interactions between negatively charged lipids and biologically relevant cations such as calcium is of a great importance. Recent combination of spectroscopic experiments, biochemical assays, and molecular simulations showed that binding of calcium to  $\text{PIP}_2$  lipids inhibits their recognition by a phospholipase C, which demonstrates that not only proteins but also lipids can get involved in calcium signaling<sup>10</sup>.

Spectroscopic experiments give accurate information about the interactions between ions and PS lipids, but the data is often indirect and difficult to interpret<sup>11–20</sup>. Some studies suggest that the binding affinity of ions to negatively charged lipids is similar to that of zwitterionic lipids, and that the amount of bound ions increases only due to the increased cation concentration in the vicinity of the membrane<sup>21,22</sup>. On the other hand, calcium forms

dehydrated complexes with PS headgroups which cause phase separation<sup>11,12,16–20,23</sup>. Theories about the interaction between calcium and PS are difficult to evaluate experimentally, especially at physiological ion concentrations, which are typically too low to yield measurable effects.

More recently, classical molecular dynamics (MD) simulations have been used to support the interpretation of spectroscopic experiments, but the results strongly depend on the force field parameters<sup>23–27</sup>. For instance, the moieties of PS lipids that interact with calcium cations vary greatly. In simulations with the CHARMM36 force field<sup>28,29</sup> using the NBfix parameters for calcium<sup>30</sup>, calcium ions interact only with the carboxylate group of PS lipids<sup>27</sup>. However, the same force field without the NBfix parameters, gives a significant binding affinity also to the phosphate region<sup>26</sup>. On the other hand, simulations with the Berger force field<sup>31,32</sup> suggest a significant calcium binding also to the carbonyls in the acyl chains<sup>25</sup>.

The NMRlipids project ([nmrlipids.blogspot.fi](http://nmrlipids.blogspot.fi)) has recently demonstrated that such controversies can be resolved by using the headgroup order parameters of phosphatidyl-choline (PC) lipids<sup>33,34</sup>, which can be related to cation binding affinity to lipid bilayers using the electrometer concept<sup>35–37</sup>. The main advantage of this approach is the direct comparison between experimental and calculated order parameters, which reduce the ambiguity arising from the interpretation of the data. Unfortunately, none of the readily available force fields was sufficiently accurate to correctly reproduce the cation binding affinity to zwitterionic PC bilayers<sup>33</sup> or to the mixtures with negatively charged PS lipids<sup>34</sup>. In our recent work<sup>38</sup>, we were able to improve the cation binding affinity to zwitterionic 1-palmitoyl-2-oleoyl-sn-glycero-3-phosphocholine (POPC) lipid bilayer by implicitly including electronic polarizability using the electronic continuum correction (ECC)<sup>39</sup>. The good agreement between the resulting ECC-POPC model and experiments enables a more detailed molecular interpretation of the calcium binding to a POPC lipid bilayer.

Here, we extend the ECC approach also to the negatively charged 1-palmitoyl-2-oleoyl-

*sn*-glycero-3-phospho-L-serine (POPS) lipid. We also complement the available experimental data for the force field quality evaluation by measuring the acyl chain C–H bond order parameters of POPS in bilayer using natural abundance  $^{13}\text{C}$  NMR. In addition to the acyl chain order parameters measured here, the quality of the newly developed ECC-POPS force field parameters is evaluated using previously published C–H bond order parameters of glycerol backbone and headgroup in various ionic conditions and lipid molar fractions<sup>19,34</sup>, as well as X-ray scattering form factors<sup>24</sup>. The overall improvement of the force field accuracy upon applying ECC paves the way to more realistic MD simulations of both neutral and negatively charged lipid bilayers for a wide range of applications.

## 2 Methods

### 2.1 Electronic continuum correction for PS lipids

Electrostatic interactions between charges in a dielectric medium are attenuated by a factor equal to the corresponding relative permittivity (dielectric constant). Standard non-polarizable force fields are capable to account for the dielectric response from the orientation of the solvent molecules (low-frequency nuclear response), but fail to account for the electronic (high frequency) polarization. In most biologically relevant environments this high frequency dielectric constant is approximately 2 (for water the value is 1.78). This means that for a non-polarizable force field that would strictly account only for the low-frequency dielectric response interactions between charges in aqueous environments should be further attenuated by a factor of 1.78, which is mathematically equivalent by scaling the charges by a factor of 0.75<sup>39,40</sup>. This electronic continuum correction (ECC), which can be view as a mean-field continuum way for accounting for electronic polarization, has been shown to significantly improve the description of interactions between aqueous ions and biologically relevant charged groups<sup>38,41–46</sup>. This correction is particularly important for high charge density species where it helps to remove artifacts such as excessive ion pairing in water<sup>41,47</sup>.

One should, however, bear in mind that existing non-polarizable force fields have been parameterized also using experimental data, which means that they may to a certain extent include implicitly electronic polarization effects. Therefore, in such cases a charge scaling factor between 0.75 and 1 should carefully be adjusted such that the electronic polarization effects are not overaccounted. In addition to the charge, the Lennard-Jones parameter  $\sigma$  of the ions needed to be modified to improve the description of hydration properties of ions with respect to scattering data in these studies by scaling with a factor  $0.72 < f_\sigma \leq 1$ . The reason for the small readjustment of the ionic radii is that the original force fields were often developed such that the first peak on the experimental ion-water oxygen radial distribution function was reproduced. Upon charge scaling this peak typically moved to slightly larger distances and the agreement with experiment was then restored by a small decrease of the Lennard-Jones  $\sigma$  parameter.

Before the ECC theory was rigorously derived, similar idea was already employed in early classical MD simulations of lipids and surfactants using the ad hoc scaling factor of 0.5 for atomic charges<sup>48–50</sup>. In our recent work, we applied the ECC to the Amber based lipid14 force field of zwitterionic POPC lipid<sup>51</sup> by scaling the partial charges and Lennard-Jones  $\sigma$  parameters of headgroup, glycerol backbone, and carbonyl regions<sup>38</sup>. The scaling factors were optimized to reproduce the calcium binding affinity to POPC lipid bilayers, evaluated using the headgroup order parameters and the electrometer concept<sup>33,35–37</sup>, and the X-ray scattering form factor without additional ions<sup>52</sup>, which resulted to the scaling factor values of  $f_q = 0.8$  and  $f_\sigma = 0.89^{38}$ .

Here, we apply the ECC to the Amber Lipid17 parameters of POPS<sup>53</sup> (available in AmberTools18<sup>54</sup>). Because POPS is anionic at physiological pH  $\approx 7$  carrying a physical total charge as aqueous ions, we apply the scaling factor derived for ions<sup>39</sup>  $f_q = 0.75$  to the partial charges of POPS in the headgroup, glycerol backbone, and carbonyl regions. The POPS lipids with a total charge of -0.75 are also neutralized by the counterion charges of +0.75 in simulations with ECC-ions<sup>55–57</sup>. Following our previous work for POPC, we use

the scaling factor  $f_\sigma = 0.89$  for the Lennard-Jones  $\sigma$  parameters to scale the corresponding parameters of atoms in the headgroup, glycerol backbone, and carbonyl regions<sup>38</sup>. Further optimization of parameters was not done in this work. The generated ECC-POPS parameters are openly available for download from Ref. 58.

## 2.2 Measurements of acyl chain order parameters

A R-type Proton Detected Local Field (R-PDLF) experiment was performed to determine C–H bond order parameters

$$S_{\text{CH}} = \frac{1}{2} \langle 3 \cos^2 \theta - 1 \rangle, \quad (1)$$

where  $\theta$  denotes the angle of the C–H bond with the bilayer normal and the angular brackets define a time average on a time scale of approximately 1 microsecond. The experiment was done using a Bruker Avance III 400 spectrometer operating at a <sup>1</sup>H Larmor frequency of 400.03 MHz equipped with a standard 4 mm CP-MAS HXY probe. The set up of the R-PDLF experiment was the following (using the notation from figures 1c and 2c in the original publication describing the R-PDLF experiment<sup>59</sup>). The magic angle spinning (MAS) frequency used was 5.15 kHz. The recoupling pulses in the R18 blocks had therefore a length of 10.79  $\mu$ s, which correspond to a nutation frequency of 46.35 kHz. Increments of  $18 \times 2$  recoupling pulses were used giving a spectral width of 2.6 kHz in the indirect dimension and a total number of 32 points in the indirect dimension were recorded. These settings enable to record dipolar slices with a C–H bond order parameter resolution of  $\pm 0.01$ . The C–H bond order parameter determined from a given dipolar splitting,  $\Delta\nu$  (see e.g. Fig. S3 in supplementary information) is equal to  $\Delta\nu/(0.315 \times 21.5 \text{ kHz})$ , where 0.315 is the scaling factor of the R18 recoupling sequence and 21.5 kHz is the maximum <sup>1</sup>H-<sup>13</sup>C dipolar coupling for a C–H bond. The refocused-INEPT transfer<sup>60,61</sup> was used for transferring the polarization from <sup>1</sup>H nuclei to the covalently bonded <sup>13</sup>C nuclei with the delays of  $\tau_1 = 1.94$  ms and  $\tau_2 = 0.97$  ms (set as multiples of the MAS rotation period). The pulses for the refocused-

INEPT sequence had a nutation frequency equal to 63.45 kHz. For acquiring the spectra, a total number of 1024 transients were recorded for each point in the indirect dimension, using an acquisition time of 0.1 s under SPINAL64  $^1\text{H}$  decoupling<sup>62</sup> with a nutation frequency of 50 kHz, and with dwell time giving a spectral width of 200 ppm for the  $^{13}\text{C}$  chemical shift dimension. The set of free induction decays recorded were then processed as described e.g. in Ref. 63. The dipolar splittings in the crowded spectral region between 29 and 30 ppm were assigned based on the previous assignments for POPC<sup>64</sup> and the POPS order parameters calculated from simulations in this work.

As in our previous work<sup>34</sup>, the sample was prepared by first mixing POPS powder (1-palmitoyl-2-oleoyl-sn-glycero-3-phospho-L-serine, purchased from Avanti Polar Lipids as sodium salt) with water (lipid:water 60:40 wt-%) in an Eppendorf tube. The mixture was repeatedly centrifuged and stirred (approximately 5 to 6 times) until a homogeneous viscous fluid was visually observed. Then 20 mg of the sample was transferred to an NMR insert suitable for 4 mm NMR rotors. Experiments were done at 298 K.

## 2.3 Simulation details

MD simulations of POPC:POPS lipid bilayers with different molar ratios and ion concentrations ( $\text{K}^+$ ,  $\text{Na}^+$ ,  $\text{Ca}^{2+}$  and  $\text{Cl}^-$ ) were performed in an orthorhombic simulation box with periodic boundary conditions using the GROMACS 2018<sup>65</sup> simulation package. The simulated systems are listed in Table 1 and the used simulation parameters in Table S1 in supplementary information. All simulations were ran for a minimum of 1  $\mu\text{s}$  at 298 K, and the first 50 ns were omitted as an equilibration period. Generated trajectories and parameter files are available from Refs. 58,66–70.

In the reference simulations with the standard Amber force field, the Lipid14 parameters<sup>51</sup> for POPC, the Lipid17 parameters for POPS<sup>53</sup>, the TIP3P water model<sup>71</sup>, and ion models by Dang and coworkers<sup>72–74</sup> were used. The previously generated<sup>75</sup> Lipid14 parameters for POPC in Gromacs format were downloaded from Ref. 76. The Lipid17 parameters

Table 1: List of MD simulations reporting their respective lipid composition, used counterions, added buffer concentrations, amounts of individual molecules, and the deployed models. The fatty acid chains for all lipids are palmitoyl (*sn*-1) and oleoyl (*sn*-2).

PC:PS ratio	counterion	added buffer conc. / mM				no. molecules		simulated with	
		K <sup>+</sup>	Na <sup>+</sup>	Ca <sup>2+</sup>	Cl <sup>-</sup>	H <sub>2</sub> O	PC:PS	ECC-lipids	Lipid17
only PS	K <sup>+</sup>	0	0	0	0	3600	0:72	•	•
only PS	Na <sup>+</sup>	0	0	0	0	3600	0:72	•	•
1:1	K <sup>+</sup>	0	0	0	0	5253	64:64	•	•
1:1	Na <sup>+</sup>	0	0	0	0	5253	64:64	•	•
4:1	K <sup>+</sup>	0	0	0	0	3600	48:12	•	-
4:1	Na <sup>+</sup>	0	0	0	0	3600	48:12	•	-
5:1	K <sup>+</sup>	0	0	0	0	3600	60:12	•	•
5:1	Na <sup>+</sup>	0	0	0	0	3600	60:12	•	•
5:1	Na <sup>+</sup>	0	0	78	78	3561	60:12	•	•
5:1	Na <sup>+</sup>	0	0	125	125	3561	60:12	•	•
5:1	Na <sup>+</sup>	0	0	202	202	3561	60:12	•	•
5:1	Na <sup>+</sup>	0	0	409	409	3522	60:12	•	•
5:1	Na <sup>+</sup>	0	0	621	621	3483	60:12	•	•
5:1	Na <sup>+</sup>	0	621	0	621	3483	60:12	•	•
5:1	Na <sup>+</sup>	0	1510	0	1510	3377	60:12	•	•
5:1	Na <sup>+</sup>	0	3002	0	3002	3213	60:12	•	•
5:1	Na <sup>+</sup>	621	0	0	621	3483	60:12	•	•
5:1	Na <sup>+</sup>	1510	0	0	1510	3377	60:12	•	•
5:1	Na <sup>+</sup>	3002	0	0	3002	3213	60:12	•	•
10:1	K <sup>+</sup>	0	0	0	0	3600	60:6	•	-
10:1	Na <sup>+</sup>	0	0	0	0	3600	60:6	•	-

for POPS were obtained from AmberTools18<sup>54</sup> and converted to Gromacs format using acpype<sup>77</sup>. The ion model by Dang and coworkers<sup>72–74</sup> was used with Amber lipids because the default Amber ion parameters, derived by Åqvist<sup>78</sup>, led to the artificial clustering of ions in solution<sup>34</sup>.

In the ECC-lipids simulations, we used the ECC-POPC parameters<sup>38</sup> (available from Ref. 79), the ECC-POPS parameteres derived in this work (see above for details and Ref. 58 for parameters), the SPC/E<sup>80</sup> water model, and ECC-ions<sup>55–57</sup>. The SPC/E water model was selected because its lower dielectric constant is consistent with the ECC concept<sup>40,81</sup>.

The C–H bond order parameters were calculated directly from Eq. 1 using a Python code openly available at Ref. 82 (`scripts/calcOrderParameters.py`) that uses the MDAnalysis library<sup>83,84</sup>. The time average was first calculated for each lipid, and the standard error of the mean from these individual values was then used as the error estimate<sup>34,75,85</sup>. The ion number density profiles were calculated using the `gmx density` tool of the Gromacs sofware package<sup>86</sup>. The salt concentrations in a buffer before solvating the lipids, as reported in the used experimental data set<sup>19</sup>, were calculated as  $[\text{salt}] = N_c \times [\text{water}] / N_w$ , where  $N_c$  is the number of additional cations,  $N_w$  is the number of water molecules, and  $[\text{water}] = 55.5 \text{ M}$ . As discussed in our previous work<sup>34</sup>, the hydration levels of multilamellae are expected to be sufficiently similar in the used simulations and reference experiments<sup>19</sup>.

## 3 Results and Discussion

### 3.1 ECC-POPS improves agreement in experimental structural parameters of a pure POPS bilayer

The X-ray scattering form factors and C–H bond order parameters from NMR experiments are good measures to validate the lipid bilayer structure in MD simulations against experiments because they are related to the bilayer dimensions (area per molecule and thickness) and conformational fluctuations of individual lipids, respectively, and can be directly cal-

culated from MD simulations<sup>85</sup>. The X-ray scattering form factors and C–H bond order parameters in the headgroup and glycerol backbone region of a POPS lipid bilayer are already available in the literature<sup>24,34</sup>. Here, we measure also the C–H bond order parameters of the acyl chain region from multi-lamellar POPS vesicles using <sup>1</sup>H–<sup>13</sup>C dipolar recoupling 2D NMR spectroscopy. As described in the Methods section, we performed R-PDLF 2D spectroscopy<sup>59</sup> to obtain spectra correlating chemical shifts (direct dimension) and C–H bond dipolar couplings (indirect dimension) from which the C–H bond order parameters defined in eq. 1 can be determined. The assignment of the peaks in the <sup>13</sup>C chemical shift dimension to acyl chain carbon sites was done based on previous work<sup>64</sup> and is shown in Figs. S1 and S2. The dipolar splittings for the assigned carbons that were used to calculate their C–H bond order parameter magnitudes are shown in Fig. S3. Because the complete assignment of the peaks in the crowded spectral region between 29–31 ppm was not possible due to the chemical shift overlap of different carbons (Fig. S2), we partially assigned the acyl chain order parameters of this region to mimic the profile predicted by the MD simulations (Fig. 1).

The Lipid17/Dang simulation gives discrepancies with the experimental X-ray form factor, larger acyl chain order parameters, and smaller area per molecule than the experimental values (Fig. 1), indicating that this simulation predicts a too compact POPS lipid bilayer. The ECC-POPS simulation gives better agreement with experiments for the X-ray scattering form factors and acyl chain order parameters (Fig. 1), indicating that the bilayer dimensions and acyl chain conformations are well described by the force field. The area per lipid from ECC-POPS simulation is slightly smaller than the value reported from SDP model<sup>24</sup> (Fig. 1), but the values agree within their error estimates. Both the smaller order parameters and larger area in ECC-POPS compared to Lipid17/Dang simulation can be explained by increased headgroup repulsion due to lower counterion binding affinity (Fig. 2). This explains also the larger area per molecule ( $57 \text{ \AA}^2$ ) reported for Lipid17 POPS simulations with Åqvist ion parameters<sup>34</sup>. However, the Dang ion parameters are used here to analyze the effect of

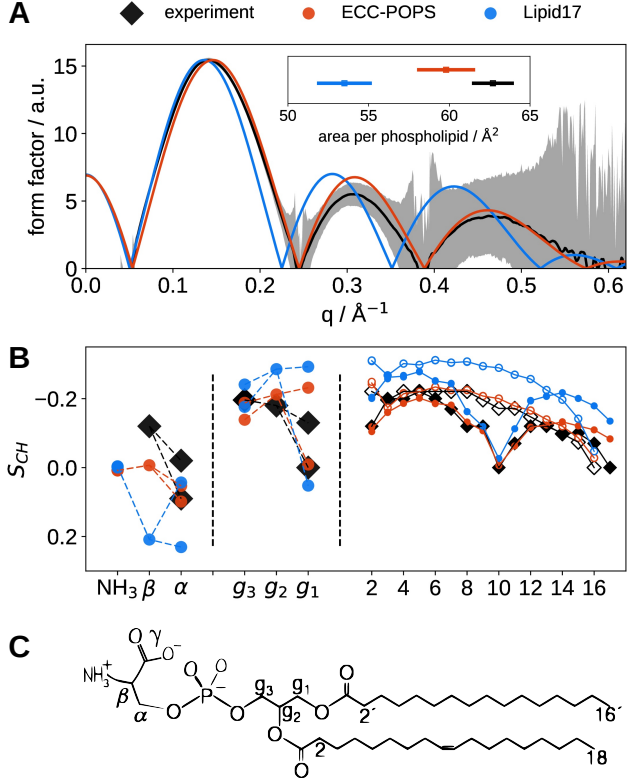


Figure 1: (A) X-ray scattering form factors and area per phospholipid of a POPS bilayer from simulations with Lipid17/Dang<sup>53,74</sup> and ECC-POPS/ECC-ions<sup>57,87</sup> compared with experiments<sup>24</sup> at 298 K. (B) Order parameters of POPS headgroup, glycerol backbone and acyl chains from the same simulations compared with experiments at 298 K.<sup>34</sup> Open/closed symbols are used for palmitoyl/oleoyl chains of POPS. (C) Chemical structure of POPS and labeling of carbon segments.

ECC to the properties of a POPS lipid bilayer because Åqvist ion parameters produce known artifacts, like artificial aggregation of ions at larger salt concentrations<sup>34,56,88</sup>.

Despite the success in simulating bilayer dimensions and acyl chain conformations, lipid force fields have typically problems in capturing the correct glycerol backbone and headgroup order parameters and conformations<sup>34,75,85</sup>. This is the case also for Lipid17 POPS simulations, where the headgroup and glycerol backbone order parameters are quite far from experimental values with Dang (Fig. 1), Åqvist and Joung-Cheatham ion parameters<sup>34</sup>. The values from ECC-POPS simulation are closer, but not in full agreement with experiments (Fig. 1).

In conclusion, the structural quality of ECC-POPS is similar to the other currently avail-

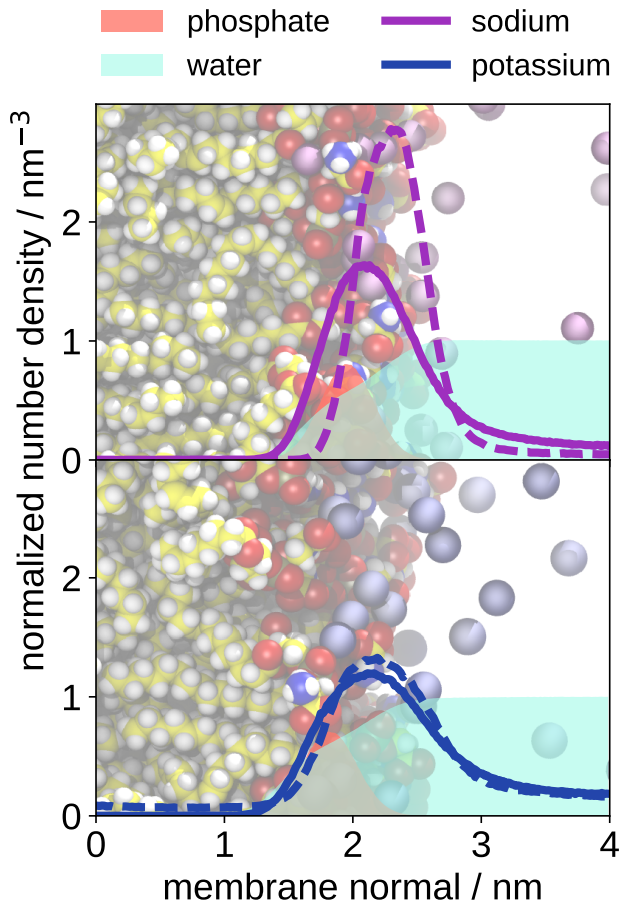


Figure 2: Number density profiles of  $\text{K}^+$  and  $\text{Na}^+$  counterions along the membrane normal axis in ECC-lipids (solid lines) and Lipid17/Dang (dashed lines) simulations of pure POPS bilayers. The density profiles of phosphate groups and water are divided by 4 and 100, respectively.

able lipid force fields<sup>33,34,75,87</sup>, giving good agreement with experiments for acyl chain conformations and bilayer dimensions, while there is a room for improvement in the glycerol backbone and headgroup region conformations.

### 3.2 Binding of counterions to POPS and POPC and interactions between their headgroups

Binding affinity of monovalent ions to lipid bilayers depends strongly on force field parameters in simulations<sup>33,34</sup>. The cation binding affinities to lipid bilayers in simulations have been previously evaluated against experiments using the order parameters of  $\alpha$  and  $\beta$  carbons in the phosphatidylcholine (PC) lipid headgroup (see Fig. 3 for the labeling)<sup>33,34,38</sup>. According to the "electrometer concept"<sup>37</sup>, these order parameters decrease proportionally to the amount of bound positive charge because the headgroup dipole tilts more parallel to the membrane normal. Although the response of PS lipid headgroup order parameters to the bound charge is also systematic, it is less well understood and the addition of cations may cause phase transitions in negatively charged bilayers<sup>17–20</sup>. Therefore, the cation binding affinity to bilayers with PS lipids has been evaluated by measuring the decrease of PC headgroup order parameters from POPC:POPS (5:1) mixtures upon addition of salt concentration, which correlate with the amount of bound cations to lipid bilayer according to the electrometer concept<sup>19,33–37</sup>. Because the evaluation of monovalent ion binding affinity to bilayers with PS lipids is complicated by the lack of ion-free state (counterions are always present with negatively charged lipids), we evaluate the counterion binding affinity to POPC:POPS mixtures also by monitoring the response of POPC headgroup order parameters to the increasing molar fraction of PS lipids<sup>34</sup> (Fig. 4).

In experiments, the addition of  $K^+$  ions led to a very modest decrease of POPC headgroup order parameters in POPC:POPS (5:1) mixture, while the decrease was more pronounced with  $Li^+$  ions and was strongest with divalent  $Mg^{2+}$  and  $Ca^{2+}$  ions<sup>19</sup>, suggesting that the binding affinity increases in order  $K^+ < Li^+ < Mg^{2+} < Ca^{2+}$ . The small changes of POPC

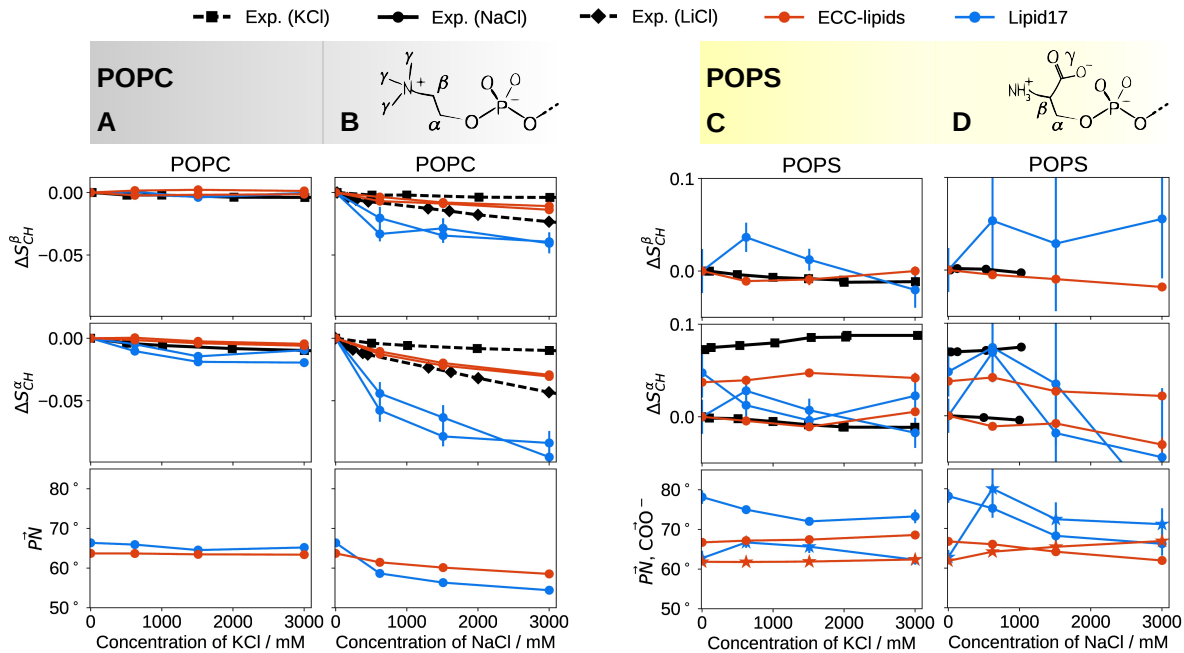


Figure 3: Changes of the headgroup order parameters, and the angles of P–N and  $\text{C}_\beta$ – $\text{C}_\gamma$  (stars) vectors with respect to the membrane normal of POPC (A, B) and POPS (C, D) in a POPC:POPS (5:1) bilayer as a function of KCl and NaCl concentration from ECC-lipids and Lipid17/Dang simulations compared with experimental values from Ref. 19 (signs from Refs. 89 and 34) at 298 K. Because experimental data with NaCl is not available for POPC, the data for KCl and LiCl (B, dashed lines) are shown as lower and upper bounds, respectively, for the response to NaCl. The y-axis for the  $\alpha$ -carbon results of POPS (C and D, middle) is shifted with the same value for both order parameters such that the lower order parameter value from pure POPS is at zero to correctly illustrate the significant forking. Error bars are not visible for ECC-lipids simulations because they are smaller than the point size. Inset in A shows the labeling of carbon segments in a POPC headgroup. For the ion density profiles, see Fig. S5 in supplementary information.

headgroup order parameters with increasing amount of KCl are close to experiments in both force fields (Fig. 3 A). The slightly overestimated change of the  $\alpha$ -carbon order parameter in the Lipid17/Dang simulations may be due to the deeper penetration of  $K^+$  into the bilayer (Fig. 4 A). Experimental data with the additional amount of  $Na^+$  in POPC:POPS (5:1) mixture is not available, but  $Li^+$  and  $K^+$  results give the lower and the upper bounds, respectively, to the sodium binding affinity (Fig. 3 B). In ECC-lipids simulations, the response of POPC headgroup order parameters to the additional sodium is close to the experimental results for lithium, while in Lipid17/Dang simulations the response is larger. Overall, the results suggest that the  $Na^+$  binding affinity is clearly overestimated in Lipid17/Dang simulations and slightly overestimated in ECC-lipids simulations, while the binding affinity of potassium is better described by both force fields. This conclusion is also supported by the POPC headgroup responses to the increasing amount of POPS in different simulations (Fig 4). In experiments, the headgroup order parameters of PC lipids increase upon addition of negatively charged PS lipids, as predicted by the electrometer concept<sup>37,90</sup>. This is the case also in simulations with the exception of Lipid17/Dang with  $Na^+$  counterions, where the stronger counterion binding affinity cancels the influence of negatively charged lipids and the increase in PC headgroup order parameters is not observed.

The behaviour of POPS headgroup can be further characterized by monitoring its order parameters in different lipid mixtures and ionic conditions (Figs. 3 and S4)<sup>19,34</sup>. In experiments, the headgroup order parameters of POPS are almost unchanged upon increasing the POPC content or monovalent ion concentration, while in Lipid17/Dang simulations the changes of POPS headgroup order parameters with increasing amount of both POPC or monovalent salts (KCl and NaCl) are overestimated (Figs. 3 and S4). Similar results are reported also for other force fields.<sup>34</sup> In ECC-lipids simulations, the response of POPS headgroup order parameters to both POPC and monovalent salt concentration (KCl and NaCl) are more modest and closer to experiments. The changes in order parameters can be related to the orientations of the P–N and  $C_\beta$ – $C_\gamma$  vectors in POPC and POPS, which change much

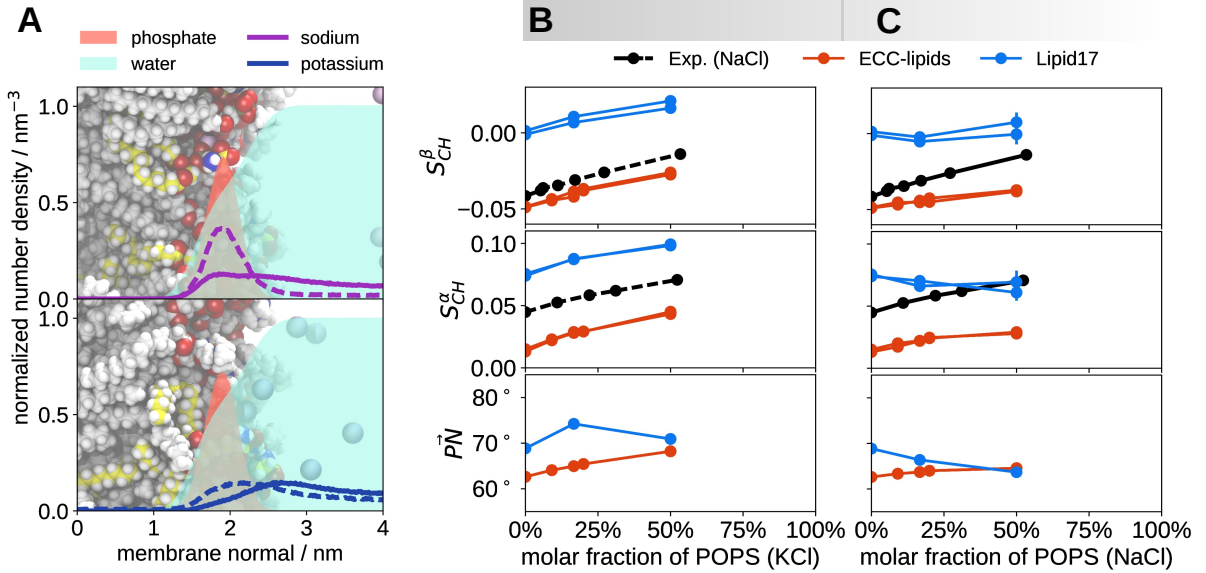


Figure 4: (A) Number density profiles of  $K^+$  and  $Na^+$  counterions along the membrane normal axis in ECC-lipids (solid lines) and Lipid17/Dang (dashed lines) simulations of POPC:POPS (5:1) bilayers. The density profiles of phosphate groups and water are divided by 4 and 100, respectively. (B, C) The POPC headgroup order parameters and the P–N vector angle with respect to the membrane normal as a function of POPS content in a bilayer from ECC-lipids and Lipid17/Dang simulations with  $K^+$  (B) and  $Na^+$  (C) counterions. Experimental order parameter values with  $Na^+$  are from Ref. 90 and the signs from Ref. 89. Because experimental values with  $K^+$  are not available, the data with  $Na^+$  is shown with dashed lines in (B). Error bars are not visible for most of the simulation points because they are smaller than the point size. Chemical structure and labelling of carbon segments of POPC is shown in Fig. 3.

less and more systematically in ECC-lipids than in Lipid17/Dang simulations (Figs. 3 and S4).

We quantify the influence of negatively charged POPS on the counterion binding affinity by comparing the relative surface excesses with respect to water,  $\Gamma_{\text{ion}}^w$ , between POPC:POPS (5:1) mixture and pure POPC in ECC-lipids simulations with currently the most realistic cation binding affinities<sup>38</sup>. The value of  $\Gamma_{\text{Na}}^w = -0.11 \pm 0.01 \text{ nm}^{-2}$  for 1 M sodium in pure ECC-POPC simulation was reported in the previous work<sup>38</sup>. The presence of ~17% POPS in a POPC bilayer increases the value to  $\Gamma_{\text{Na}}^w = 0.092 \pm 0.005 \text{ nm}^{-2}$  for 0.621 M sodium, while value for potassium remains negative,  $\Gamma_{\text{K}}^w = -0.123 \pm 0.005 \text{ nm}^{-2}$  in POPC:POPS (5:1) mixture (Fig. S5). The increase in sodium binding affinity upon addition of anionic POPS is not expected to depend on the slightly overestimated  $\text{Na}^+$  binding in ECC-lipid simulations, because the inaccuracy is similar for pure POPC (Fig 3 in Ref. 38) and POPC:POPS (5:1) mixture (Fig. 3).

### 3.3 Molecular interaction and binding affinity of $\text{Ca}^{2+}$ cations to mixed POPC:POPS (5:1) membrane

Our recent work demonstrates that the POPC headgroup order parameters measured from POPC:POPS (5:1) mixture as a function of  $\text{CaCl}_2$  concentration can be used to evaluate the calcium binding affinity to lipid bilayers containing PS lipids<sup>19,34</sup>. The decrease of the PC headgroup order parameters in this mixture upon addition of  $\text{CaCl}_2$  were overestimated by the Lipid17/Dang simulations (Fig. 5) and all other tested force fields except CHARMM36 with the recently introduced NBfix parameters for calcium<sup>30,91</sup>, which underestimated the headgroup order parameter response. In ECC-lipids simulations, the headgroup responses are in better agreement with experiments, indicating that the lower binding affinity than in Lipid17/Dang simulations is more realistic (Fig. 5). Therefore, we use ECC-lipids simulations to quantify the influence of negatively charged POPS on calcium binding affinity to lipid bilayers. The relative surface excess of calcium with respect to water  $\Gamma_{\text{Ca}}^w = 0.09 \text{ nm}^{-2}$  for pure

POPC bilayer with 467 mM CaCl<sub>2</sub><sup>79</sup> is increased to  $\Gamma_{Ca}^w = 0.24\text{nm}^{-2}$  for the POPC:POPS (5:1) bilayer with 409 mM CaCl<sub>2</sub>. At these concentrations, the total amount of lipids per bound Ca<sup>2+</sup> is ~ 5.4 in the pure POPC system and ~ 4.8 in the POPC:POPS (5:1) mixture. Also, the residence times of Ca<sup>2+</sup> at the membrane are 3-4 times longer in POPC:POPS (5:1) mixture (Fig. S7) than in pure POPC<sup>38</sup>. Besides lower binding affinity, ECC-lipids simulations yield smaller error bars for order parameters and shorter residence times (Fig. S7) than those typically observed in simulations with other force fields<sup>34,38,92</sup>, suggesting that the ECC accelerates the equilibration of ions at lipid bilayer interface. Therefore, our 1  $\mu\text{s}$  simulations are sufficiently long for the ECC-lipids simulations, because 90% of the calcium residence times are shorter than 60 ns for pure POPC bilayer and shorter than 200 ns for POPC:POPS (5:1) mixture, while the longest observed residence times are 141 ns and 485 ns, respectively (Fig. S7).

Interactions between Ca<sup>2+</sup> ions and PS lipids can be further characterized by monitoring the POPS headgroup order parameters from POPC:POPS (5:1) mixture with increasing CaCl<sub>2</sub> concentration<sup>19</sup>. In experiments, the headgroup order parameters of POPS exhibit a strong dependence on low CaCl<sub>2</sub> concentrations with a rapid saturation below 100 mM (Fig. 5)<sup>19</sup>. These changes are overestimated in simulations with Lipid17/Dang (Fig. 5) and other tested force fields in our recent work<sup>34</sup>, including CHARMM36 with the NBfix corrections for calcium which underestimated the binding affinity. In ECC-lipids simulations, the changes of the PS headgroup order parameters are not overestimated, but the strong dependence on low concentrations of CaCl<sub>2</sub> is not fully reproduced (Fig. 5). In addition to possibly suboptimal interactions between calcium ions and PS headgroup, the potential sources of this discrepancy include the above observed slight overestimation of Na<sup>+</sup> counterions and imperfect structures of the lipid headgroup (Fig. 1).

Recent analyzes of interaction sites between calcium and PS lipids combining MD simulations with various experimental techniques have been controversial because the results strongly depend on force fields parameters<sup>25-27,34</sup>. Here, we analyze the calcium binding de-

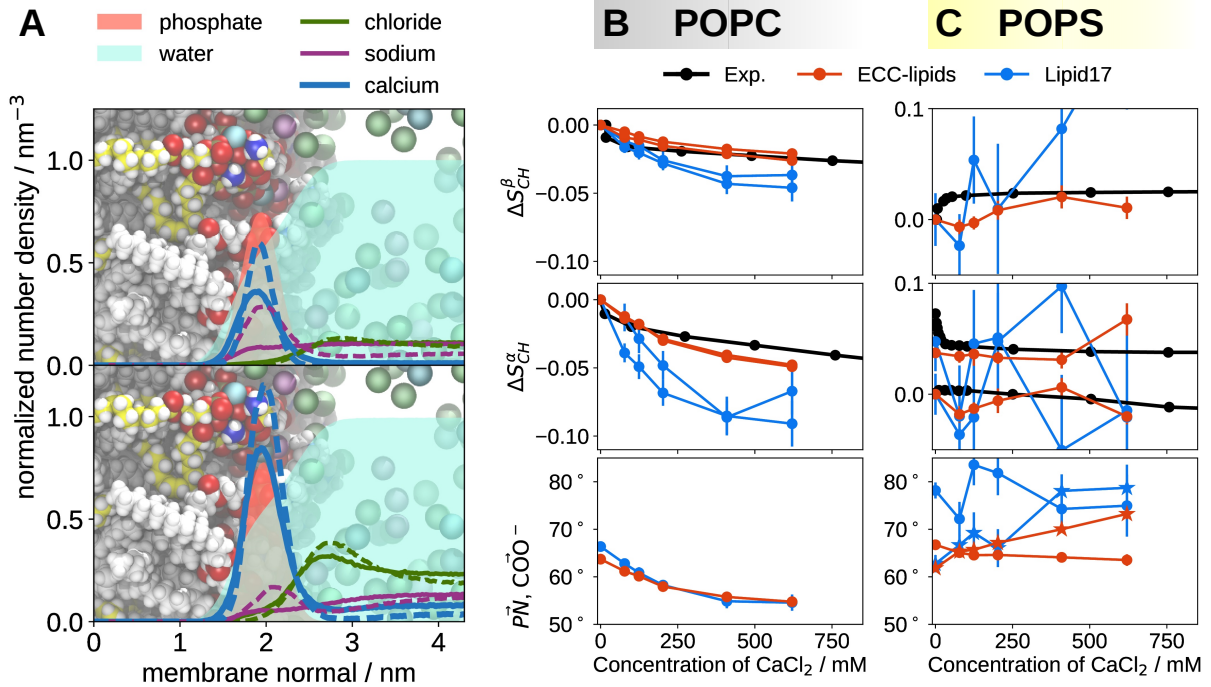


Figure 5: (A) Number density profiles of Ca<sup>2+</sup> and Cl<sup>-</sup> ions and Na<sup>+</sup> counterions along the normal of POPC:POPS (5:1) bilayer with 80 mM (A, top) and 200 mM (A, bottom) of CaCl<sub>2</sub> from simulations with ECC-lipids (solid) and Lipid17 (dashed). The Ca<sup>2+</sup>, phosphate and water densities are divided by 2, 4 and 100, respectively. (B, C) Changes of the headgroup order parameters, and the angles of P–N (circles) and C <sub>$\beta$</sub> –C <sub>$\gamma$</sub>  (stars) vectors with respect to the membrane normal of POPC (B) and POPS (C) in a POPC:POPS (5:1) bilayer as a function of CaCl<sub>2</sub> from ECC-lipids and Lipid17/Dang simulations compared with experimental values from Ref. 19 (signs from Refs. 89 and 34) at 298 K. The y-axis for the  $\alpha$ -carbon results of POPS (C, right) is shifted with the same value for both order parameters such that the lower order parameter value from pure POPS is at zero to correctly illustrate the significant forking. Error bars are not visible for ECC-lipids simulations because they are smaller than the point size.

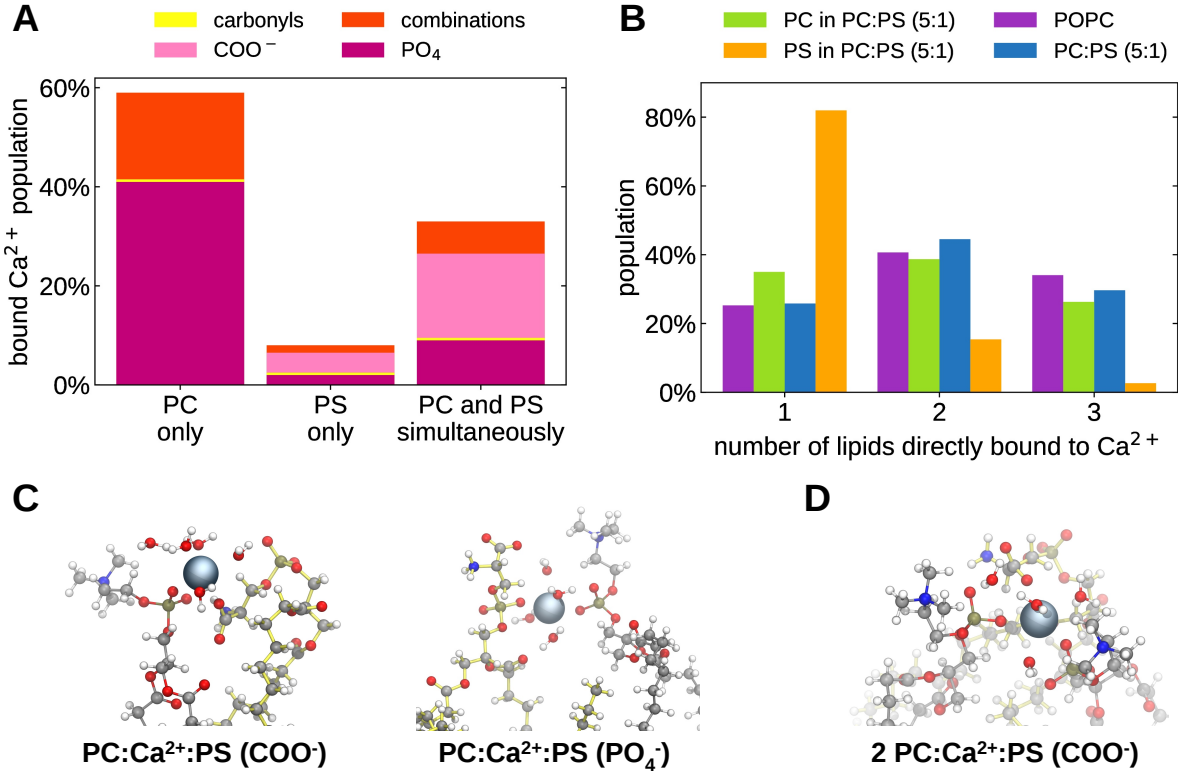


Figure 6: **(A)** Percentages of the bound  $\text{Ca}^{2+}$  in exclusive contact with the given oxygen moiety when bound to PC only, PS only or simultaneously to both calculated from ECC-lipids simulation of POPC:POPS (5:1) bilayer with 409 mM  $\text{CaCl}_2$ . In the case of simultaneous binding to both PC and PS, the percentages refer to the moieties in PS. For numerical values, see table S2. **(B)** Relative probabilities of  $\text{Ca}^{2+}$  ions to coordinate with the given number of lipids in a pure POPC bilayer with 350 mM  $\text{CaCl}_2$  and in POPC:POPS (5:1) mixture with 400 mM  $\text{CaCl}_2$ . Analysis was done for both systems by considering all lipids (blue and violet) and for POPC:POPS (5:1) mixture also by considering only POPC and POPS lipids separately (green and orange). Clusters of four or more lipids were not observed in either membrane. The threshold for counting coordinated lipids in a complex with  $\text{Ca}^{2+}$  was set to 0.3 nm, for the distance between the cation and the oxygen atoms of the lipids. **(C and D)** Representative example configurations of  $\text{Ca}^{2+}$  coordinated complexes of one POPS with one (C) or two POPC lipids (D). More configurations are shown in Fig. S6 in the SI. Previously published simulation data for pure POPC bilayers<sup>38</sup> were taken directly from Ref. 79.

tails of POPC:POPS (5:1) mixture with 409 mM CaCl<sub>2</sub> from ECC-lipids simulations, which surpass the quality of other force fields in direct comparison with experimental order parameters. In the ECC-lipid simulation, calcium ions binds approximately twice more likely to the carboxylate than to the phosphate moiety of POPS headgroup, while binding only to acyl chain carbonyls is almost negligible (Fig. 6 and Table S2). The result is consistent with CHARMM36 simulations without the NBfix correction<sup>26</sup>, but CHARMM36 simulations with the NBfix correction<sup>30</sup> predict almost exclusive binding to carboxylate group<sup>27</sup> and Berger simulations show significant binding affinity also to acyl chain carbonyls<sup>25</sup>. On the other hand, calcium ions bind too strongly on bilayers simulated using CHARMM36 without the NBfix correction or Berger models, and too weakly on CHARMM36 bilayers with the NBfix correction<sup>33,34</sup>. Furthermore, in CHARMM36 simulations without the NBfix, calcium ions coordinate with even four distinct PS lipids<sup>26</sup>, while coordination with more than two PS lipids is very rare in our ECC-lipids simulations (Fig. 6).

The improved accuracy in ECC-lipids simulations motivates also the more detailed analysis of POPS headgroup response to the bound calcium ions, which is potentially important in calcium regulated lipid-protein interactions<sup>2</sup>. Upon addition of 620 mM CaCl<sub>2</sub> to POPC:POPS (5:1) mixture, the average orientation of P–N vectors in both POPC and POPS headgroups tilts more perpendicular to the membrane surface by 11° and 3°, respectively, in ECC-lipids simulations (Fig. 5), suggesting that the PS headgroup orientation is less sensitive to the bound calcium than PC. On the other hand, the average orientation of the C<sub>β</sub>–C<sub>γ</sub> vector in PS headgroup tilts to the opposite direction by 11° in the same system, probably due to the attraction between COO<sup>−</sup> groups and cations adsorbed at the phosphate region.

## 4 Conclusions

We have applied ECC to implicitly include electronic polarization to the Amber Lipid17 force field parameters of negatively charged POPS lipid. Because PS headgroup bears a unit

negative charge, we apply the scaling factor of 0.75, derived for monovalent ions<sup>39</sup>, to the partial charges in the headgroup, glycerol backbone and carbonyl regions of POPS. Following our previous work for zwitterionic POPC lipids, the Lennard-Jones  $\sigma$  parameters of the same POPS segments were scaled by a factor of 0.89 to optimize the hydration properties of the bilayer<sup>38</sup>. Similarly to other state of the art lipid models, the created ECC-POPS parameters give lipid bilayer dimensions and acyl chain structures in agreement with experiments, but leaves room for improvement for the headgroup structure when validated against NMR and scattering experiments<sup>75,85</sup>. Nevertheless, ECC-lipid parameters describe cation ( $\text{Na}^+$  and  $\text{Ca}^{2+}$ ) binding affinities and their interactions with PS headgroups better than other available lipid force fields, when validated using the headgroup order parameters and “electrometer concept”<sup>34</sup>. There is, however, still room for improvement in capturing the sensitive headgroup responses to small concentrations of  $\text{CaCl}_2$ .

In our ECC-lipids simulation,  $\text{Ca}^{2+}$  ions bind twice more likely to carboxylate groups of PS headgroups than to phosphate groups, while binding only to carbonyls is negligible. However, calcium can bind also to carbonyls when simultaneously bound also to carboxylate (Fig. S6) or phosphate group. Binding of  $\text{Ca}^{2+}$  ions to more than two POPS lipids simultaneously is very rare in ECC-lipids simulations. Because ECC-lipids parameters give the best results in direct comparison with NMR order parameters, we believe that our results help in resolving controversial interpretations of more indirect experiments using different force fields<sup>25–27</sup> and demonstrate the usefulness of ECC also for membranes with charged lipids. Furthermore, the present simulations pave the way for more realistic MD simulations of biomolecular systems with anionic membranes allowing to elucidate signaling processes involving PS and  $\text{Ca}^{2+}$ .

The general philosophy behind our approach is to build upon existing non-polarizable force fields making the minimum of necessary changes by scaling only groups bearing a sizeable (partial) charge, followed by slight readjustments of van der Waals radii and possibly also other parameters such as those concerning dihedral angle terms. The present

work thus represents another piece in the mosaic that leads to development of an improved empirical force field for biomolecular simulations involving aqueous salt solutions, proteins, peptides, lipid membranes, and/or nucleic acids, which include electronic polarization effects in a mean field way via charge scaling without extra computational costs compared to standard non-polarizable simulations. We believe that such ECC force fields will be useful in modeling complex biomembranes when simulations with explicitly polarizable force fields for biomolecules<sup>93-95</sup> are not practical.

## Acknowledgement

P.J. acknowledges support from the Czech Science Foundation via an EXPRO grant no. 19-26854X. Computational resources were supplied by the Ministry of Education, Youth and Sports of the Czech Republic under the Projects CESNET (Project No. LM2015042) and CERIT-Scientific Cloud (Project No. LM2015085) provided within the program Projects of Large Research, Development and Innovations Infrastructures. O.H.S.O. acknowledges financial support from Academy of Finland (315596), Integrated Structural Biology Research Infrastructure of Helsinki Institute of Life Science (Instruct-HiLIFE), and CSC-IT center for science for computational resources.

## Supporting Information Available

The following files are available free of charge.

- SI.pdf: Measured 1D and 2D NMR spectra, additional details and results from simulations about monovalent ion binding, configurations and populations of bound calcium to POPS lipids, and residence times of bound calcium.

This material is available free of charge via the Internet at <http://pubs.acs.org/>.

## References

- (1) Lemmon, M. A. *Nat. Rev. Mol. Cell Biol.* **2008**, *9*, 99–111.
- (2) Leventis, P. A.; Grinstein, S. *Annu. Rev. Biophys.* **2010**, *39*, 407–427.
- (3) Li, L.; Shi, X.; Guo, X.; Li, H.; Xu, C. *Trends Biochem. Sci.* **2014**, *39*, 130 – 140.
- (4) Yeung, T.; Gilbert, G. E.; Shi, J.; Silvius, J.; Kapus, A.; Grinstein, S. *Science* **2008**, *319*, 210–213.
- (5) Zhao, H.; Tuominen, E. K. J.; Kinnunen, P. K. J. *Biochemistry* **2004**, *43*, 10302–10307.
- (6) Gorbenko, G. P.; Kinnunen, P. K. *Chem. Phys. Lipids* **2006**, *141*, 72 – 82.
- (7) Wilschut, J.; Duezguenes, N.; Papahadjopoulos, D. *Biochemistry* **1981**, *20*, 3126–3133.
- (8) Papahadjopoulos, D.; Nir, S.; Düzungünes, N. *J. Bioenerg. Biomembr.* **1990**, *22*, 157–179.
- (9) Verma, S. K.; Leikina, E.; Melikov, K.; Gebert, C.; Kram, V.; Young, M. F.; Uygur, B.; Chernomordik, L. V. *J. Biol. Chem.* **2018**, *293*, 254–270.
- (10) Bilkova, E.; Pleskot, R.; Rissanen, S.; Sun, S.; Czogalla, A.; Cwiklik, L.; Rög, T.; Vattulainen, I.; Cremer, P. S.; Jungwirth, P.; Coskun, Ü. *J. Am. Chem. Soc.* **2017**, *139*, 4019–4024.
- (11) Hauser, H.; Finer, E.; Darke, A. *Biochem. Biophys. Res. Commun.* **1977**, *76*, 267 – 274.
- (12) Kurland, R. J. *Biochem. Biophys. Res. Commun.* **1979**, *88*, 927 – 932.
- (13) Eisenberg, M.; Gresalfi, T.; Riccio, T.; McLaughlin, S. *Biochemistry* **1979**, *18*, 5213–5223.
- (14) Hauser, H.; Shipley, G. G. *Biochemistry* **1983**, *22*, 2171–2178.

- (15) Dluhy, R.; Cameron, D. G.; Mantsch, H. H.; Mendelsohn, R. *Biochemistry* **1983**, *22*, 6318–6325.
- (16) Hauser, H.; Shipley, G. *Biochim. Biophys. Acta* **1985**, *813*, 343 – 346.
- (17) Feigenson, G. W. *Biochemistry* **1986**, *25*, 5819–5825.
- (18) Mattai, J.; Hauser, H.; Demel, R. A.; Shipley, G. G. *Biochemistry* **1989**, *28*, 2322–2330.
- (19) Roux, M.; Bloom, M. *Biochemistry* **1990**, *29*, 7077–7089.
- (20) Roux, M.; Bloom, M. *Biophys. J.* **1991**, *60*, 38 – 44.
- (21) Seelig, J. *Cell Biol. Int. Rep.* **1990**, *14*, 353–360.
- (22) Sinn, C. G.; Antonietti, M.; Dimova, R. *Colloids Surf. A* **2006**, *282-283*, 410 – 419.
- (23) Boettcher, J. M.; Davis-Harrison, R. L.; Clay, M. C.; Nieuwkoop, A. J.; Ohkubo, Y. Z.; Tajkhorshid, E.; Morrissey, J. H.; Rienstra, C. M. *Biochemistry* **2011**, *50*, 2264–2273.
- (24) Pan, J.; Cheng, X.; Monticelli, L.; Heberle, F. A.; Kučerka, N.; Tielemans, D. P.; Katsaras, J. *Soft Matter* **2014**, *10*, 3716–3725.
- (25) Melcrová, A.; Pokorná, Š.; Pullanchery, S.; Kohagen, M.; Jurkiewicz, P.; Hof, M.; Jungwirth, P.; Cremer, P. S.; Cwiklik, L. *Sci. Rep.* **2016**, *6*, 38035.
- (26) Hallock, M. J.; Greenwood, A. I.; Wang, Y.; Morrissey, J. H.; Tajkhorshid, E.; Rienstra, C. M.; Pogorelov, T. V. *Biochemistry* **2018**, *57*, 6897–6905.
- (27) Valentine, M. L.; Cardenas, A. E.; Elber, R.; Baiz, C. R. *Biophys. J.* **2018**, *115*, 1541 – 1551.
- (28) Klauda, J. B.; Venable, R. M.; Freites, J. A.; O'Connor, J. W.; Tobias, D. J.; Mondragon-Ramirez, C.; Vorobyov, I.; Jr, A. D. M.; Pastor, R. W. *J. Phys. Chem. B* **2010**, *114*, 7830–7843.

- (29) Venable, R. M.; Luo, Y.; Gawrisch, K.; Roux, B.; Pastor, R. W. *J. Phys. Chem. B* **2013**, *117*, 10183–10192.
- (30) Kim, S.; Patel, D.; Park, S.; Slusky, J.; Klauda, J.; Widmalm, G.; Im, W. *Biophys. J.* **2016**, *111*, 1750 – 1760.
- (31) Berger, O.; Edholm, O.; Jähnig, F. *Biophys. J.* **1997**, *72*, 2002 – 2013.
- (32) Mukhopadhyay, P.; Monticelli, L.; Tielemans, D. P. *Biophys. J.* **2004**, *86*, 1601 – 1609.
- (33) Catte, A.; Girych, M.; Javanainen, M.; Loison, C.; Melcr, J.; Miettinen, M. S.; Monticelli, L.; Maatta, J.; Oganesyan, V. S.; Ollila, O. H. S.; Tynkkynen, J.; Vilov, S. *Phys. Chem. Chem. Phys.* **2016**, *18*, 32560–32569.
- (34) Antila, H. S.; Buslaev, P.; Favela-Rosales, F.; Mendes Ferreira, T.; Gushchin, I.; Javanainen, M.; Kav, B.; Madsen, J. J.; Melcr, J.; Miettinen, M. S.; Määttä, J.; Nencini, R.; Ollila, O. H. S.; Piggot, T. J. *J. Phys. Chem. B* **2019**, *123*, 9066–9079.
- (35) Akutsu, H.; Seelig, J. *Biochemistry* **1981**, *20*, 7366–7373.
- (36) Altenbach, C.; Seelig, J. *Biochemistry* **1984**, *23*, 3913–3920.
- (37) Seelig, J.; MacDonald, P. M.; Scherer, P. G. *Biochemistry* **1987**, *26*, 7535–7541.
- (38) Melcr, J.; Martinez-Seara, H.; Nencini, R.; Kolafa, J.; Jungwirth, P.; Ollila, O. H. S. *J. Phys. Chem. B* **2018**, *122*, 4546–4557.
- (39) Leontyev, I. V.; Stuchebrukhov, A. A. *J. Chem. Phys.* **2009**, *130*, 085102.
- (40) Leontyev, I. V.; Stuchebrukhov, A. A. *J. Chem. Phys.* **2014**, *141*, 014103.
- (41) Pluhařová, E.; Mason, P. E.; Jungwirth, P. *J. Phys. Chem. A* **2013**, *117*, 11766–11773.
- (42) Kohagen, M.; Mason, P. E.; Jungwirth, P. *J. Phys. Chem. B* **2014**, *118*, 7902–7909.
- (43) Kohagen, M.; Lepšík, M.; Jungwirth, P. *J. Phys. Chem. Lett.* **2014**, *5*, 3964–3969.

- (44) Xie, W. J.; Zhang, Z.; Gao, Y. Q. *J. Phys. Chem. B* **2016**, *120*, 2343–2351.
- (45) Kroutil, O.; Předota, M.; Kabeláč, M. *J. Mol. Model.* **2017**, *23*, 327.
- (46) Bruce, E. E.; van der Vegt, N. F. A. *J. Chem. Phys.* **2018**, *148*, 222816.
- (47) Vazdar, M.; Jungwirth, P.; Mason, P. E. *J. Phys. Chem. B* **2013**, *117*, 1844–1848.
- (48) Jönsson, B.; Edholm, O.; Teleman, O. *J. Chem. Phys.* **1986**, *85*, 2259–2271.
- (49) Egberts, E.; Marrink, S.-J.; Berendsen, H. J. C. *Eur. Biophys. J.* **1994**, *22*, 423–436.
- (50) López Cascales, J. J.; García de la Torre, J.; Marrink, S. J.; Berendsen, H. J. C. *J. Chem. Phys.* **1996**, *104*, 2713.
- (51) Dickson, C. J.; Madej, B. D.; Skjevik, A. A.; Betz, R. M.; Teigen, K.; Gould, I. R.; Walker, R. C. *J. Chem. Theory Comput.* **2014**, *10*, 865–879.
- (52) Kučerka, N.; Nieh, M. P.; Katsaras, J. *Biochim. Biophys. Acta* **2011**, *1808*, 2761–2771.
- (53) Gould, I.; Skjevik, A.; Dickson, C.; Madej, B.; Walker, R. Lipid17: A Comprehensive AMBER Force Field for the Simulation of Zwitterionic and Anionic Lipids. 2018; In preparation.
- (54) Case, D. A.; Ben-Shalom, I.; Brozell, D.; Cerutti, S.R.; Darden, T. A.; Cheatham, T. r.; Simmerling, C. L.; Wang, J.; Duke, R. E.; Luo, R.; Crowley, M.; Roitberg, A.; Walker, R. C.; Zhang, W.; Kollman, P. Amber 2018. 2018; <http://ambermd.org/index.php>.
- (55) Pluhařová, E.; Fischer, H. E.; Mason, P. E.; Jungwirth, P. *Mol. Phys.* **2014**, *112*, 1230–1240.
- (56) Kohagen, M.; Mason, P. E.; Jungwirth, P. *J. Phys. Chem. B* **2016**, *120*, 1454–1460.

- (57) Martínek, T.; Duboué-Dijon, E.; Timr, Š.; Mason, P. E.; Baxová, K.; Fischer, H. E.; Schmidt, B.; Pluhařová, E.; Jungwirth, P. *J. Chem. Phys.* **2018**, *148*, 222813.
- (58) Melcr, J. Molecular dynamics simulations of lipid bilayers containing POPC and POPS (5:1) with ECC-lipids force field, and Na<sup>+</sup> (K<sup>+</sup>) counterions at various additional concentrations of NaCl and KCl. 2019; <https://doi.org/10.5281/zenodo.3332778>.
- (59) Dvinskikh, S. V.; Zimmermann, H.; Maliniak, A.; Sandstrom, D. *J. Magn. Reson.* **2004**, *168*, 194–201.
- (60) Morris, G. A.; Freeman, R. *J. Am. Chem. Soc.* **1979**, *101*, 760–762.
- (61) Burum, D.; Ernst, R. *J. Magn. Res.* **1980**, *39*, 163 – 168.
- (62) Fung, B.; Khitrin, A.; Ermolaev, K. *J. Magn. Res.* **2000**, *142*, 97 – 101.
- (63) Ferreira, T. M.; Medronho, B.; Martin, R. W.; Topgaard, D. *Phys. Chem. Chem. Phys.* **2008**, *10*, 6033–6038.
- (64) Ferreira, T. M.; Coreta-Gomes, F.; Ollila, O. H. S.; Moreno, M. J.; Vaz, W. L. C.; Topgaard, D. *Phys. Chem. Chem. Phys.* **2013**, *15*, 1976–1989.
- (65) Abraham, M. J.; Murtola, T.; Schulz, R.; Páll, S.; Smith, J. C.; Hess, B.; Lindah, E. *SoftwareX* **2015**, *1-2*, 19–25.
- (66) Melcr, J. Molecular dynamics simulations of lipid bilayers containing POPC and POPS (5:1) with ECC-lipids force field, and Na<sup>+</sup> (K<sup>+</sup>) counterions at various CaCl<sub>2</sub> additional concentrations. 2018; <https://doi.org/10.5281/zenodo.1488102>.
- (67) Melcr, J. Molecular dynamics simulations of lipid bilayers containing POPC and POPS (various mixtures) with ECC-lipids force field, and Na<sup>+</sup> (K<sup>+</sup>) counterions. 2018; <https://doi.org/10.5281/zenodo.1488094>.

- (68) Melcr, J. Molecular dynamics simulations of lipid bilayers containing POPC and POPS with the lipid17 force field, NaCl and KCl salt concentrations. 2018; <https://doi.org/10.5281/zenodo.1487895>.
- (69) Melcr, J. Molecular dynamics simulations of lipid bilayers containing POPC and POPS with the lipid17 force field and ff99 ions. 2018; <https://doi.org/10.5281/zenodo.1487906>.
- (70) Melcr, J. Molecular dynamics simulations of lipid bilayers containing POPC and POPS with the lipid17 force field, only counterions, and CaCl<sub>2</sub> concentrations. 2018; <https://doi.org/10.5281/zenodo.1487761>.
- (71) Jorgensen, W. L.; Chandrasekhar, J.; Madura, J. D.; Impey, R. W.; Klein, M. L. *J. Chem. Phys.* **1983**, *79*, 926–935.
- (72) Smith, D. E.; Dang, L. X. *J. Chem. Phys.* **1994**, *100*, 3757–3766.
- (73) Chang, T.-M.; Dang, L. X. *J. Phys. Chem. B* **1999**, *103*, 4714–4720.
- (74) Dang, L. X.; Schenter, G. K.; Glezakou, V.-A.; Fulton, J. L. *J. Phys. Chem. B* **2006**, *110*, 23644–54.
- (75) Botan, A.; Favela-Rosales, F.; Fuchs, P. F. J.; Javanainen, M.; Kanduč, M.; Kulig, W.; Lamberg, A.; Loison, C.; Lyubartsev, A.; Miettinen, M. S.; Monticelli, L.; Määttä, J.; Ollila, O. H. S.; Retegan, M.; Róg, T.; Santuz, H.; Tynkkynen, J. *J. Phys. Chem. B* **2015**, *119*, 15075–15088.
- (76) Ollila, O. H. S.; Retegan, M. MD simulation trajectory and related files for POPC bilayer (Lipid14, Gromacs 4.5). 2014; <http://dx.doi.org/10.5281/zenodo.12767>.
- (77) Sousa da Silva, A. W.; Vranken, W. F. *BMC Res. Notes* **2012**, *5*, 367.
- (78) Åqvist, J. *J. Phys. Chem.* **1990**, *94*, 8021–8024.

- (79) Melcr, J. Simulations of POPC lipid bilayer in water solution at various NaCl and CaCl<sub>2</sub> concentrations using ECC-POPC force field. 2017; <https://doi.org/10.5281/zenodo.1118266>.
- (80) Berendsen, H. J. C.; Grigera, J. R.; Straatsma, T. P. *J. Phys. Chem.* **1987**, *91*, 6269–6271.
- (81) Leontyev, I.; Stuchebrukhov, A. *Phys. Chem. Chem. Phys.* **2011**, *13*, 2613–2626.
- (82) Bacle, A.; Buslaev, P.; Cwiklik, L.; Favela, F.; Ferreira, T.; Fuchs, P.; Gushchin, I.; Javanainen, M.; Kav, B.; Madsen, J.; Melcr, J.; Miettinen, M.; Nencini, R.; Ollila, S.; Papadopoulos, C.; Piggot, T. MATCH GitHub repository. <https://github.com/NMRLipids/MATCH>.
- (83) Michaud-Agrawal, N.; Denning, E. J.; Woolf, T. B.; Beckstein, O. *J. Comput. Chem.* **2011**, *32*, 2319–2327.
- (84) Richard J. Gowers,; Max Linke,; Jonathan Barnoud,; Tyler J. E. Reddy,; Manuel N. Melo,; Sean L. Seyler,; Jan Domski,; David L. Dotson,; Sébastien Buchoux,; Ian M. Kenney,; Oliver Beckstein, MDAnalysis: A Python Package for the Rapid Analysis of Molecular Dynamics Simulations. Proceedings of the 15th Python in Science Conference. 2016; pp 98 – 105.
- (85) Ollila, O. S.; Pabst, G. *Biochim. Biophys. Acta* **2016**, *1858*, 2512 – 2528.
- (86) Abraham, M.; van der Spoel, D.; Lindahl, E.; Hess, B.; the GROMACS development team, GROMACS user manual version 5.0.7. 2015.
- (87) Pluháčková, K.; Kirsch, S. A.; Han, J.; Sun, L.; Jiang, Z.; Unruh, T.; Böckmann, R. A. *J. Phys. Chem. B* **2016**, *120*, 3888–3903.
- (88) Chen, A. A.; ; Pappu, R. V. *J. Phys. Chem. B* **2007**, *111*, 11884–11887.

- (89) Ferreira, T. M.; Sood, R.; Bärenwald, R.; Carlström, G.; Topgaard, D.; Saalwächter, K.; Kinnunen, P. K. J.; Ollila, O. H. S. *Langmuir* **2016**, *32*, 6524–6533.
- (90) Scherer, P.; Seelig, J. *EMBO J.* **1987**, *6*, 2915–2922.
- (91) Han, K.; Venable, R. M.; Bryant, A.-M.; Legacy, C. J.; Shen, R.; Li, H.; Roux, B.; Gericke, A.; Pastor, R. W. *J. Phys. Chem. B* **2018**, *122*, 1484–1494.
- (92) Javanainen, M.; Melcrová, A.; Magarkar, A.; Jurkiewicz, P.; Hof, M.; Jungwirth, P.; Martinez-Seara, H. *Chem. Commun.* **2017**, *53*, 5380–5383.
- (93) Shi, Y.; Xia, Z.; Zhang, J.; Best, R.; Wu, C.; Ponder, J. W.; Ren, P. *J. Chem. Theory Comput.* **2013**, *9*, 4046–4063.
- (94) Li, H.; Chowdhary, J.; Huang, L.; He, X.; MacKerell, A. D.; Roux, B. *J. Chem. Theory Comput.* **2017**, *13*, 4535–4552.
- (95) Chu, H.; Peng, X.; Li, Y.; Zhang, Y.; Li, G. *Molecules* **2018**, *23*.

# Graphical TOC Entry

